

**Supporting Information for
Stable Silicon(II) Monohydride**

Anukul Jana, Dirk Leusser, Ina Objartel, Herbert W. Roesky,* and Dietmar Stalke*

*To whom correspondence should be addressed.

Email: hroesky@gwdg.de (HWR) and dstalke@chemie.uni-goettingen.de (DS)

This PDF file includes:

Charge Density Distribution

References

Charge Density Distribution

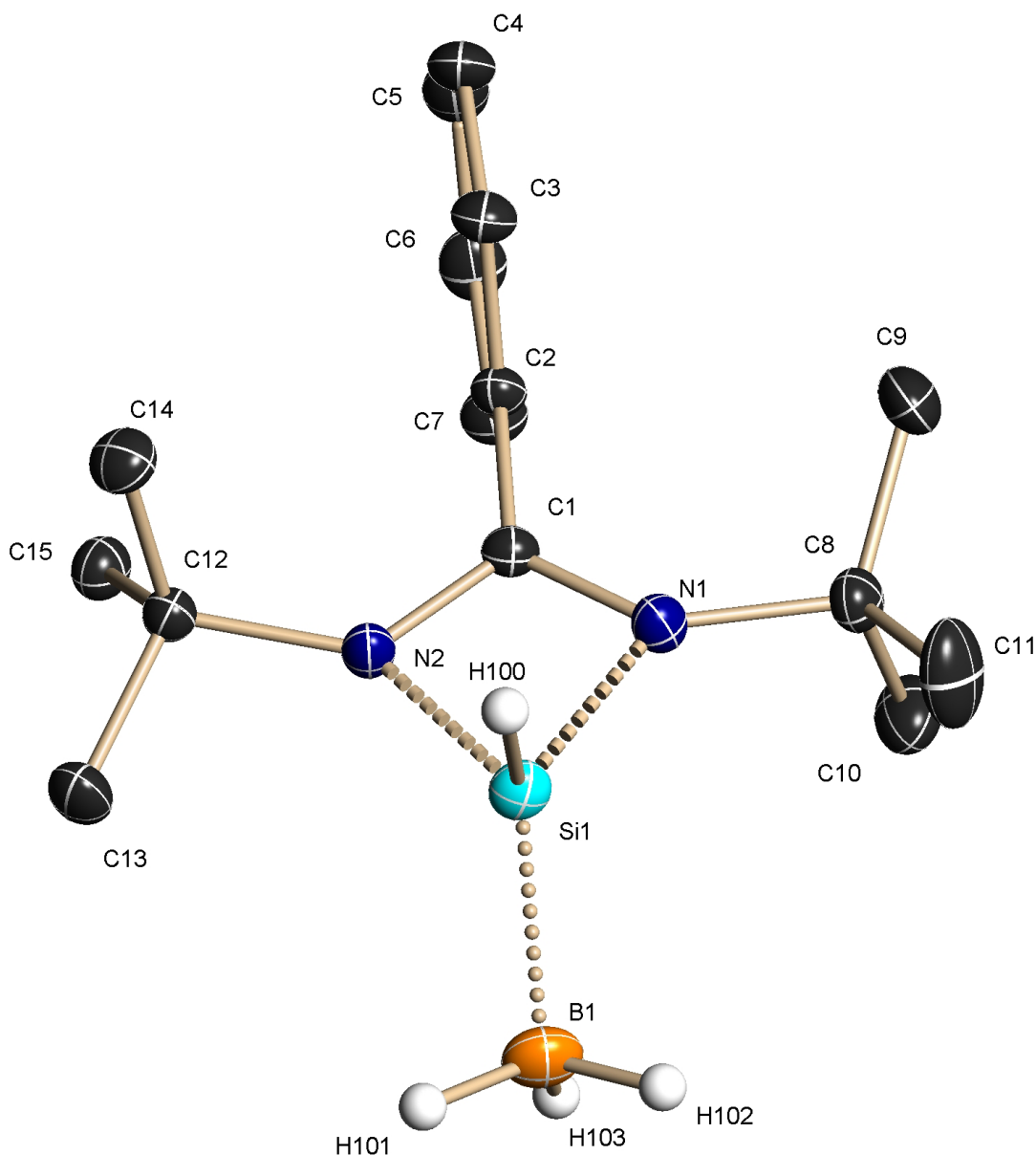


Figure S1: Molecular structure of $\text{PhC}(\text{Nt-Bu})_2\text{SiH}(\text{BH}_3)$ (**3**)

1 Data collection / Integration / Absorption Correction

The high-resolution data for the multipole refinement were collected in an omega-scan mode ($\Delta\omega = 0.3^\circ$) at fixed φ -angles with a detector distance of 5 cm (low and mid-order data) and 4 cm (high-order data) at exposure times between 10 (low-order) and 180s (high-order data). This procedure led to a high-resolution data set (for

details see Table S1), which was corrected for absorption, scaled and merged with the new SADABS-2008/2^[S1] version, which was modified by the author for charge density data purposes. Friedel pairs were not included in the merging process to take the anomalous dispersion in the chiral space group $P2_12_12_1$ into account.

The structure was solved with SHELXS^[S2] and a conventional Independent Atom Model (IAM) refinement using all data was performed with SHELXL^[S3] to check the data quality and to determine the absolute structure. The refined IAM served as the starting model for the subsequent multipole refinement.

The following strategy was applied: the positional and anisotropic displacement parameters of the non-hydrogen atoms were refined with the high-order data ($d_{\max} = 0.60 \text{ \AA}$). These parameters were kept fixed during the subsequent refinement steps. The hydrogen atoms were identified by a difference Fourier analysis using the low-order data ($d_{\min} = 1.00 \text{ \AA}$). Based on the same subset of data, the hydrogen atom positions were refined with a SADI-restraint for the boron-bound hydrogen atoms and an isotropic riding model (default values of SHELXL) for the sp³- (methyl, BH_3) and sp²-bound hydrogen atoms was applied. Then the hydrogen atoms were shifted along their bonding vectors to distances of 1.085 \AA for those bound to sp³-hybridized carbon atoms, 1.076 \AA for those bound to sp²-hybridized carbon atoms, 1.200 \AA for the BH_3 , and 1.480 \AA for H100, which is bonded to the silicon atom.^[S4, S5]

2 Multipole Refinement

The multipole refinement using the atom-centered multipole model of Hansen and Coppens^[S6] was carried out on F^2 with the full-matrix-least-squares refinement program XDLSM implemented in the XD2006^[S7] program package. Preliminary tested models led to a flat and featureless residual density distribution except a

relatively high residual density peak at the silicon position. The appearance of this peak was highly correlated to the cut-off (and the scale factor of course) for the calculation of the residual density maps. It vanished totally below $\sin \Theta/\lambda = 0.9 \text{ \AA}^{-1}$. The height of the peak was reduced during multipole refinement to about 50% of the value after IAM refinement. Even an anharmonic motion model for silicon was tested which led to a flat residual density but a non-defined Si–B bond path. Nevertheless, it has to be pointed out, that the main structural features, like Laplacian distributions, the bond critical points (except Si–B), charges, etc. were in good agreement for all convergent models. Therefore it is more a question of 'taste' which model is preferred. However, the existence of a 'ghost peak at silicon' implies the need of a sufficient scaling (2Θ -dependence) or as an alternative an adapted weighting scheme. Excessive tests by inspection of Fourier densities subsequent to the refinements, lead to the use of a weighting scheme (as defined in SHEXL) where the statistical weights were modified by $(0.05 P)^2$, with $P = [1/3 * \text{maximum of } (0 \text{ or } F_o^2) + 2/3 * F_c^2]$. This led to a very satisfying flat and featureless residual density distribution after the mutlipole refinement.

The core and the spherical valence densities were composed of relativistic Dirac-Fock wave functions reported by Su, Coppens and Macchi (SCM bank file).^[S8] Single-zeta orbitals with energy-optimized Slater exponents were used for the deformation density terms.^[S9] The deformation density terms of the silicon atom were tested to be modeled with optimized n_l values (2, 4, 6, 8 for $l = 1, 2, 3, 4$) vs. default values.^[S10] Since no significant dependence concerning the use of the scattering factor model could be detected, the default values were used for the subsequent refinements. The radial fit of these functions was optimized by refinement of the expansion-contraction parameters κ and κ' . The expansions over the spherical

harmonics were truncated at the hexadecapolar level for all hetero atoms and all multipoles ($n_l = 1$ to 4) of each atom shared the same κ' -set (*keep kappa* constraint). The deformation densities of the hydrogen atoms were represented by bond directed dipoles and quadrupoles. To derive adequate parameters for the contraction of the hydrogen atoms, κ and κ' values suggested by Volkov *et al.* were introduced and kept fixed during the refinement.^[S11] Moreover, a riding model and distance constraints were applied for the hydrogen atoms during the first steps of the multipole refinement. In the final steps of the refinement the hydrogen atoms were refined without distance and thermal motion constraints by using a low-order cut-off ($d_{\min} = 1.00 \text{ \AA}$). After each step the change of the hydrogen parameters was checked for significance. The freely, with the resolution cut-off, refined U(H) led to physically meaningful values and were therefore kept fixed during the final steps of the aspherical refinement.

Several models have been refined and compared, differing in the degree of applied chemical constraints and local non-crystallographic symmetry. A maximum amount of chemical constraints and symmetry restrictions for the multipolar functions stabilized the refinement procedures in the non-centrosymmetric space group and reduced correlations. On the other hand the model had to be flexible enough to account for small differences of supposed chemically equivalent atoms, e.g. the both chemically equivalent *t*-Bu units were treated independently, while the carbon within each butyl group were constrained. The density parameters were implemented in the refinement routines in a stepwise manner but in the final cycles all parameters except the κ' (due to the known effect of large correlations with the other multipole parameters) were refined together using all positive reflections (no $\|/\sigma$ exclusion to avoid bias) until convergence was reached. Chemically equivalent or similar atoms (methyl carbon

atoms, *o*-carbon - and *m*-carbon atoms of the phenyl ring) were constrained to share the same expansion/contraction parameters, monopole and multipole populations. Hydrogen atoms with similar chemical environment were modeled with one set of parameters each: methyl hydrogen atoms (one set for each butyl-unit); phenyl ring hydrogen atoms; and the boron bound hydrogen atoms. Several additional local non-crystallographic symmetry restrictions were applied for the angular functions (mm₂-symmetry for C1, -6m₂ for C2, *m* for the other atoms in the phenyl ring, three-fold symmetry at all carbon atoms of the *t*-Bu groups and the boron atom, cylinder symmetry for all hydrogen atoms). The multipole refinement led to a very satisfactory fit. The electron density is not biased by and well separated from the thermal motion of the non-hydrogen atoms. This was justified by the rigid bond test (DMSDA test) according to Hirshfeldt.^[S12]

2.1 Results of the DMSDA-test:

Differences of Mean-Squares Displacement Amplitudes (DMSDA) [10^4 \AA^2] along interatomic bonds [Å]

bond	bond lenght	difference	bond	bond lenght	difference
Si–N1	1.8292	1	C3–C4	1.3925	7
Si–N2	1.8284	2	C4–C5	1.3992	1
Si–B	1.9624	23	C5–C6	1.3933	-4
N1–C8	1.4743	6	C6–C7	1.3898	0
N1–C1	1.3360	4	C8–C9	1.5261	5
N2–C1	1.3434	2	C8–C10	1.5292	0
N2–C12	1.4736	12	C8–C11	1.5241	-3
C1–C2	1.4826	1	C12–C13	1.5282	2
C2–C3	1.3960	-1	C12–C14	1.5325	-2
C2–C7	1.3952	0	C12–C15	1.5329	-1

2.2 Residuals:

The final model which included just those constraints that were chemically sensible led to the lowest R -values and a flat and featureless residual density. Therefore, this model was selected for the subsequent discussion.

The final residuals were:

$$R(F) = 0.0320$$

$$Rw(F) = 0.0376$$

$$R(F^2) = 0.0399$$

$$Rw(F^2) = 0.0691$$

$$\text{GOF}_w = 0.9099 / \text{GOF} = 2.205$$

$$N_{\text{reflections}}/N_{\text{variables}} > 38 \text{ in the final cycle}$$

The final parameters of the multipole model (populations, contraction/expansion parameters) can be found in the CIF-file.

Table S1. Crystal data of 3.

Identification code	silylene
Empirical formula	C ₁₅ H ₂₇ BN ₂ Si
Formula weight	274.29
Temperature [K]	100(1)
Wavelength [Å]	0.71073
Crystal system	orthorhombic
Space group	P2 ₁ 2 ₁ 2 ₁
Unit cell dimensions [Å]	$a = 8.516(2)$ $\alpha = 90^\circ$ $b = 11.588(3)$ $\beta = 90^\circ$ $c = 17.098(5)$ $\gamma = 90^\circ$
Volume [Å ³]	1687.2(8)
Z	4
Density (calculated) [Mg/m ³]	1.080
Absorption coefficient [mm ⁻¹]	0.129
F(000)	600
Crystal size [mm]	0.16 x 0.14 x 0.10
Theta range for data collection [°]	2.12 - 49.15
Index ranges	-17 <= h <= 18, -24 <= k <= 24, -35 <= l <= 29
Reflections collected	86541
Independent reflections	15218
Completeness to theta = 49.15°	0.924
Completeness to theta = 30.0°	1.000
Absorption correction	face-indexed
Max. and min. transmission	0.9704 / 0.9131
Refinement method	full-matrix least-squares on F^2
Data / parameters	14699 / 384
Flack parameter ^[S13]	0.01(4)
wGoF on F^2 , GoF on F^2	0.9099, 2.205
Final R indices based on all data	$R(F) = 0.0320$, $Rw(F) = 0.0376$ $R(F^2) = 0.0399$, $Rw(F^2) = 0.0691$
Largest diff. peak and hole [e/ Å ³] for all data	0.306, -0.175

2.3 Bond Lengths [Å] and Angles [°]

Si(1)–N(1): 1.8292(4)	N(1)–Si(1)–N(2): 71.741(18)	C(8)–C(10)–H(10C): 109.11(4)
Si(1)–N(2): 1.8284(4)	N(1)–Si(1)–B(1): 126.25(2)	H(10A)–C(10)–H(10B): 108.83(4)
Si(1)–B(1): 1.9624(5)	N(1)–Si(1)–H(100): 103.117(15)	H(10A)–C(10)–H(10C): 108.64(5)
N(1)–C(1): 1.3360(5)	N(2)–Si(1)–B(1): 125.07(2)	H(10B)–C(10)–H(10C): 109.05(5)
N(2)–C(1): 1.3434(5)	N(2)–Si(1)–H(100): 104.301(14)	C(8)–C(11)–H(11A): 110.32(5)
C(1)–C(2): 1.4826(4)	B(1)–Si(1)–H(100): 116.991(17)	C(8)–C(11)–H(11B): 107.03(5)
C(2)–C(3): 1.3960(5)	Si(1)–N(1)–C(1): 91.09(3)	C(8)–C(11)–H(11C): 108.77(6)
C(2)–C(7): 1.3952(5)	Si(1)–N(2)–C(1): 90.89(3)	H(11A)–C(11)–H(11B): 112.80(7)
C(3)–C(4): 1.3925(6)	N(1)–C(1)–N(2): 106.24(3)	H(11A)–C(11)–H(11C): 109.82(5)
C(4)–C(5): 1.3992(9)	N(1)–C(1)–C(2): 128.16(3)	H(11B)–C(11)–H(11C): 107.97(6)
C(5)–C(6): 1.3932(8)	N(2)–C(1)–C(2): 125.59(3)	C(13)–C(12)–C(14): 109.80(3)
C(6)–C(7): 1.3898(5)	C(1)–C(2)–C(3): 118.65(3)	C(13)–C(12)–C(15): 108.83(3)
C(7)–H(7): 1.0760(4)	C(1)–C(2)–C(7): 120.76(3)	C(14)–C(12)–C(15): 110.81(3)
C(8)–C(9): 1.5261(6)	C(3)–C(2)–C(7): 120.54(3)	C(12)–C(13)–H(13A): 110.42(4)
C(8)–C(10): 1.5292(7)	C(2)–C(3)–C(4): 119.54(4)	C(12)–C(13)–H(13B): 111.22(3)
C(8)–C(11): 1.5241(7)	C(2)–C(3)–H(3): 119.80(3)	C(12)–C(13)–H(13C): 111.25(4)
C(12)–C(13): 1.5282(5)	C(4)–C(3)–H(3): 120.66(4)	H(13A)–C(13)–H(13B): 107.17(4)
C(12)–C(14): 1.5325(6)	C(3)–C(4)–C(5): 119.87(4)	H(13A)–C(13)–H(13C): 108.28(4)
C(12)–C(15): 1.5329(6)	C(3)–C(4)–H(4): 117.64(6)	H(13B)–C(13)–H(13C): 108.37(4)
Si(1)–H(100): 1.47342(11)	C(5)–C(4)–H(4): 122.48(4)	C(12)–C(14)–H(14A): 110.94(3)
B(1)–H(101): 1.2187(6)	C(4)–C(5)–C(6): 120.35(4)	C(12)–C(14)–H(14B): 111.54(4)
B(1)–H(102): 1.2298(6)	C(4)–C(5)–H(5): 118.91(6)	C(12)–C(14)–H(14C): 111.74(3)
B(1)–H(103): 1.1937(6)	C(6)–C(5)–H(5): 120.73(6)	H(14A)–C(14)–H(14B): 111.50(4)
C _{ring} –H _{ring} : 1.0760(4)	C(5)–C(6)–C(7): 119.82(5)	H(14A)–C(14)–H(14C): 106.74(4)
C _{methyl} –H _{methyl} : 1.0850(7)	C(5)–C(6)–H(6): 119.37(4)	H(14B)–C(14)–H(14C): 104.09(3)
	C(7)–C(6)–H(6): 120.73(5)	C(12)–C(15)–H(15A): 113.13(4)
	C(2)–C(7)–C(6): 119.87(4)	C(12)–C(15)–H(15B): 107.42(3)
	C(2)–C(7)–H(7): 120.51(3)	C(12)–C(15)–H(15C): 109.07(3)
	C(6)–C(7)–H(7): 119.62(4)	H(15A)–C(15)–H(15B): 110.83(3)
	C(9)–C(8)–C(10): 109.94(4)	H(15A)–C(15)–H(15C): 105.52(3)
	C(9)–C(8)–C(11): 109.75(5)	H(15B)–C(15)–H(15C): 110.91(4)
	C(10)–C(8)–C(11): 110.45(5)	Si(1)–B(1)–H(101): 100.86(3)
	C(8)–C(9)–H(9A): 110.13(4)	Si(1)–B(1)–H(102): 102.35(3)
	C(8)–C(9)–H(9B): 107.82(4)	Si(1)–B(1)–H(103): 113.33(3)
	C(8)–C(9)–H(9C): 110.16(5)	H(101)–B(1)–H(102): 111.10(4)
	H(9A)–C(9)–H(9B): 108.37(5)	H(101)–B(1)–H(103): 111.43(5)
	H(9A)–C(9)–H(9C): 108.22(5)	H(102)–B(1)–H(103): 116.37(4)
	H(9B)–C(9)–H(9C): 112.12(5)	

C(8)–C(10)–H(10A): 110.39(5)

C(8)–C(10)–H(10B): 110.78(5)

2.4 Residual Density Distribution

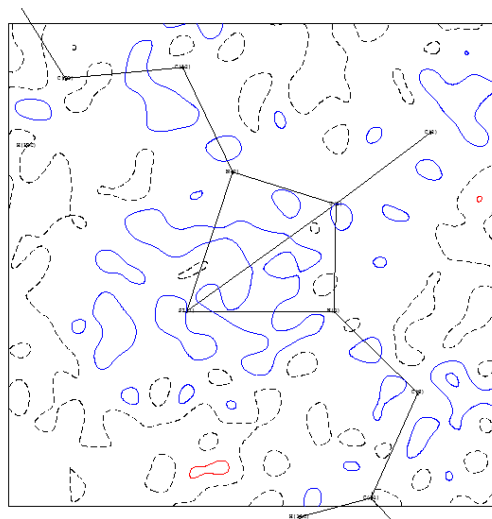
Results from the Fast Fourier Transformation (XDFFT):

$\sin \Theta/\lambda < 1.0 \text{ \AA}^{-1}$, $\|/\sigma > 3$:

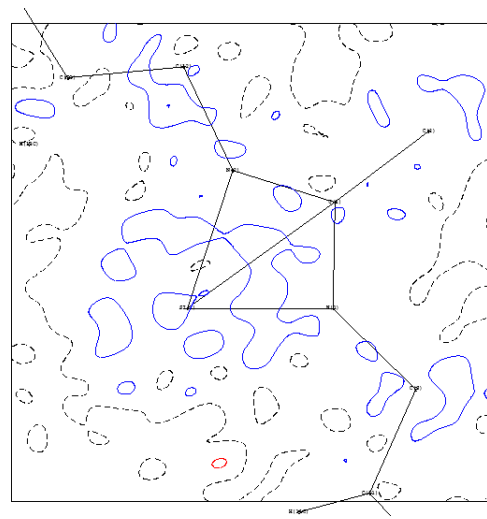
diff_density_max: 0.239 e \AA^{-3}
 diff_density_min: -0.155 e \AA^{-3}
 diff_density_rms: 0.043 e \AA^{-3}
 highest peaks: Q1 = 0.24, Q2 = 0.21 e \AA^{-3}

all data

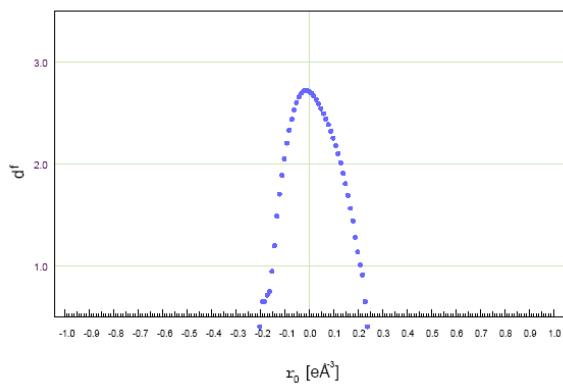
diff_density_max: 0.306 e \AA^{-3}
 diff_density_min: -0.175 e \AA^{-3}
 diff_density_rms: 0.048 e \AA^{-3}
 highest peaks: Q1 = 0.31, Q2 = 0.23 e \AA^{-3}



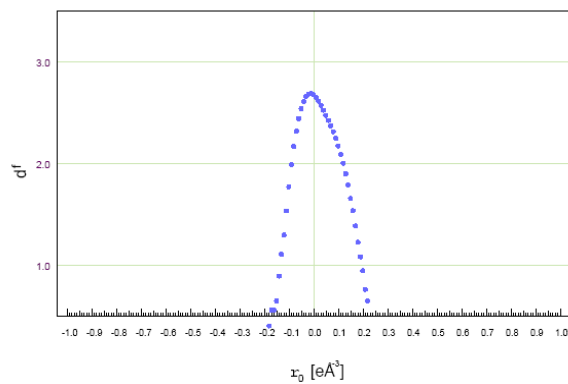
residual density in the SiN_2 -plane
 (all data, contour interval = 0.1 e \AA^{-3})



residual density in the SiN_2 -plane
 ($\sin \Theta/\lambda < 1.0 \text{ \AA}^{-1}$, contour interval = 0.1 e \AA^{-3})



fractal dimension for all data



fractal dimension for data with $\sin \Theta/\lambda < 1.0 \text{ \AA}^{-1}$

Figure S2: Residual density analysis of 3

The residual density is in very good approximation flat and featureless, which can be seen by visual inspection of the Fourier maps above or numerically by a new tool developed by K. Meindl and J. Henn.^[S14] The shape of the distribution of the fractal dimension is as required for a sufficient fit, in good approximation of gaussian type, symmetric, slim, and does not show any shoulders.

2.5 Bond Critical Points (BCPs)

bond: :λ ₁ ρ(\mathbf{r}_{BCP}) $\nabla^2\rho(\mathbf{r}_{\text{BCP}})$ BP d1 d2	bond: :λ ₁ ρ(\mathbf{r}_{BCP}) $\nabla^2\rho(\mathbf{r}_{\text{BCP}})$ BP d1 d2
SI(1) -N(1): 0.826(35) 5.172(91) 1.8430 0.8249 1.0180 -4.78 -4.03 13.98 0.19	C(9) -H(9A): 1.917(28) -19.041(78) 1.0858 0.6359 0.4498 -16.63 -14.92 12.51 0.11
SI(1) -N(2): 0.739(31) 6.101(86) 1.8336 0.8166 1.0170 -4.92 -3.75 14.77 0.31	C(9) -H(9B): 1.908(9) -19.080(37) 1.0859 0.6350 0.4509 -16.61 -14.97 12.50 0.11
SI(1) -B(1): 0.871(25) -5.066(41) 1.9655 0.9828 0.9827 -4.88 -4.43 4.25 0.10	C(9) -H(9C): 1.910(9) -18.987(37) 1.0858 0.6355 0.4503 -16.63 -14.88 12.52 0.12
SI(1) -H(100): 0.801(52) 9.015(120) 1.4803 0.7759 0.7044 -5.54 -3.69 18.24 0.50	C(10) -H(10A): 1.931(1) -19.401(0) 1.0851 0.6372 0.4479 -16.67 -15.23 12.50 0.09
N(1) -C(1): 2.524(28) -21.182(143) 1.3371 0.7697 0.5674 -20.19 -18.50 17.51 0.09	C(10) -H(10B): 1.926(1) -19.405(0) 1.0851 0.6365 0.4486 -16.66 -15.23 12.49 0.09
N(1) -C(8): 1.751(19) -10.205(72) 1.4754 0.8703 0.6051 -12.68 -12.59 15.07 0.01	C(10) -H(10C): 1.929(1) -19.387(0) 1.0852 0.6369 0.4482 -16.65 -15.24 12.50 0.09
N(2) -C(1): 2.418(27) -17.641(129) 1.3455 0.7572 0.5884 -19.25 -17.00 18.61 0.13	C(11) -H(11A): 1.923(1) -19.463(0) 1.0851 0.6356 0.4495 -16.72 -15.21 12.47 0.10
N(2) -C(12): 1.698(18) -9.201(71) 1.4755 0.8819 0.5937 -13.96 -9.99 14.75 0.40	C(11) -H(11B): 1.915(1) -19.264(0) 1.0856 0.6355 0.4501 -16.68 -15.09 12.51 0.10
C(1) -C(2): 1.921(24) -13.600(72) 1.4827 0.7547 0.7281 -14.74 -13.49 14.63 0.09	C(11) -H(11C): 1.933(1) -19.445(0) 1.0852 0.6367 0.4485 -16.67 -15.24 12.47 0.09
C(2) -C(3): 2.058(21) -13.843(68) 1.3963 0.7231 0.6732 -15.25 -12.39 13.80 0.23	C(12) -C(13): 1.760(17) -15.273(52) 1.5300 0.7107 0.8193 -13.46 -11.72 9.91 0.15
C(2) -C(7): 2.251(15) -19.341(50) 1.3960 0.6907 0.7053 -18.02 -14.98 13.65 0.20	C(12) -C(14): 1.810(14) -13.221(36) 1.5329 0.7438 0.7890 -12.62 -11.58 10.97 0.09
C(3) -C(4): 2.251(25) -19.330(81) 1.3930 0.7061 0.6868 -17.48 -14.97 13.13 0.17	C(12) -C(15): 1.780(16) -12.867(39) 1.5333 0.7340 0.7993 -12.16 -11.55 10.84 0.05
C(3) -H(3): 2.006(35) -23.084(128) 1.0761 0.6687 0.4073 -18.76 -17.71 13.38 0.06	C(13) -H(13A): 2.015(1) -22.989(0) 1.0852 0.6561 0.4290 -17.86 -17.25 12.12 0.04
C(4) -C(5): 2.373(30) -24.137(100) 1.3993 0.6832 0.7160 -20.37 -16.52 12.75 0.23	C(13) -H(13B): 1.998(1) -22.871(0) 1.0852 0.6547 0.4306 -17.91 -17.09 12.14 0.05
C(4) -H(4): 1.954(27) -21.193(80) 1.0768 0.6658 0.4109 -17.63 -16.91 13.34 0.04	C(13) -H(13C): 2.010(1) -22.948(0) 1.0852 0.6558 0.4294 -17.87 -17.21 12.13 0.04
C(5) -C(6): 2.293(37) -20.118(108) 1.3933 0.7197 0.6736 -17.44 -15.81 13.13 0.10	C(14) -H(14A): 1.962(1) -21.467(0) 1.0874 0.6585 0.4289 -17.56 -16.32 12.41 0.08
C(5) -H(5): 1.909(35) -20.749(117) 1.0763 0.6511 0.4252 -17.25 -16.08 12.58 0.07	C(14) -H(14B): 1.986(1) -22.237(0) 1.0864 0.6571 0.4293 -17.71 -16.77 12.25 0.06
C(6) -C(7): 2.158(1) -18.845(1) 1.3906 0.7179 0.6727 -17.18 -14.11 12.44 0.22	C(14) -H(14C): 1.976(1) -21.626(0) 1.0872 0.6593 0.4279 -17.59 -16.42 12.38 0.07
C(6) -H(6): 1.949(2) -21.431(1) 1.0767 0.6629 0.4138 -17.55 -16.98 13.10 0.03	C(15) -H(15A): 2.003(9) -22.897(35) 1.0852 0.6546 0.4306 -17.84 -17.14 12.08 0.04
C(7) -H(7): 2.011(0) -23.134(0) 1.0761 0.6702 0.4059 -18.84 -17.78 13.49 0.06	C(15) -H(15B): 2.006(9) -22.935(34) 1.0852 0.6543 0.4309 -17.77 -17.23 12.07 0.03
C(8) -C(9): 1.776(17) -12.332(42) 1.5267 0.7174 0.8093 -12.07 -11.09 10.83 0.09	C(15) -H(15C): 2.008(26) -22.926(80) 1.0852 0.6550 0.4301 -17.85 -17.17 12.09 0.04
C(8) -C(10): 1.843(16) -15.867(43) 1.5299 0.7179 0.8119 -13.28 -12.77 10.18 0.04	B(1) -H(101): 0.991(30) 0.332(52) 1.2195 0.5035 0.7160 -6.13 -4.22 10.68 0.45
C(8) -C(11): 1.816(18) -15.300(50) 1.5248 0.7078 0.8170 -13.33 -12.16 10.19 0.10	B(1) -H(102): 0.983(11) -0.296(50) 1.2303 0.5062 0.7241 -6.06 -4.11 9.87 0.47

B(1)	-H(103):	1.003(11)	1.756(51)	1.1976	0.4966	0.7010
		-6.79	-4.40	12.95	0.54	

All anticipated critical points could be determined and quantified. The bond critical points (BCP), (3, -1) critical points in $\rho(\mathbf{r})$, are displayed as red spheres, the ring critical point, (3, +1) critical points in $\rho(\mathbf{r})$, are displayed as yellow spheres. The connection lines between the atoms are the calculated bond paths (BP), lines of maximum density between two atoms with respect to any neighbouring line. The atoms are represented as blue spheres, (3, +3) critical points (local maxima).

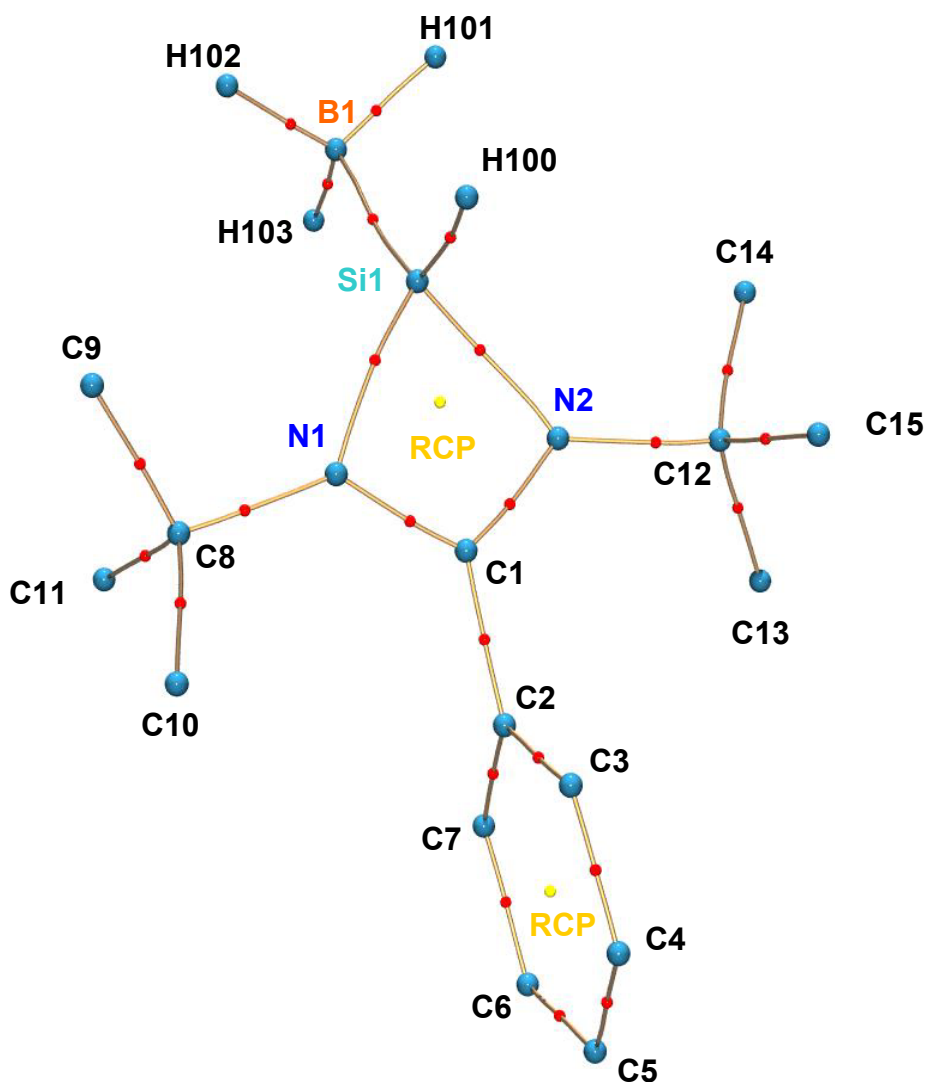


Figure S3: Molecular graph of **3**, made up by the bond paths (BP, connection lines), bond critical points (BCP, red spheres), ring critical points (yellow spheres), and local extrema of the density (atomic positions, blue spheres).

Table S2. Topological parameters of the bond critical points and integrated atomic charges with esds calculated from XDPROP; the esds for the averaged values were calculated from the minimum and maximum deviation from the mean value.

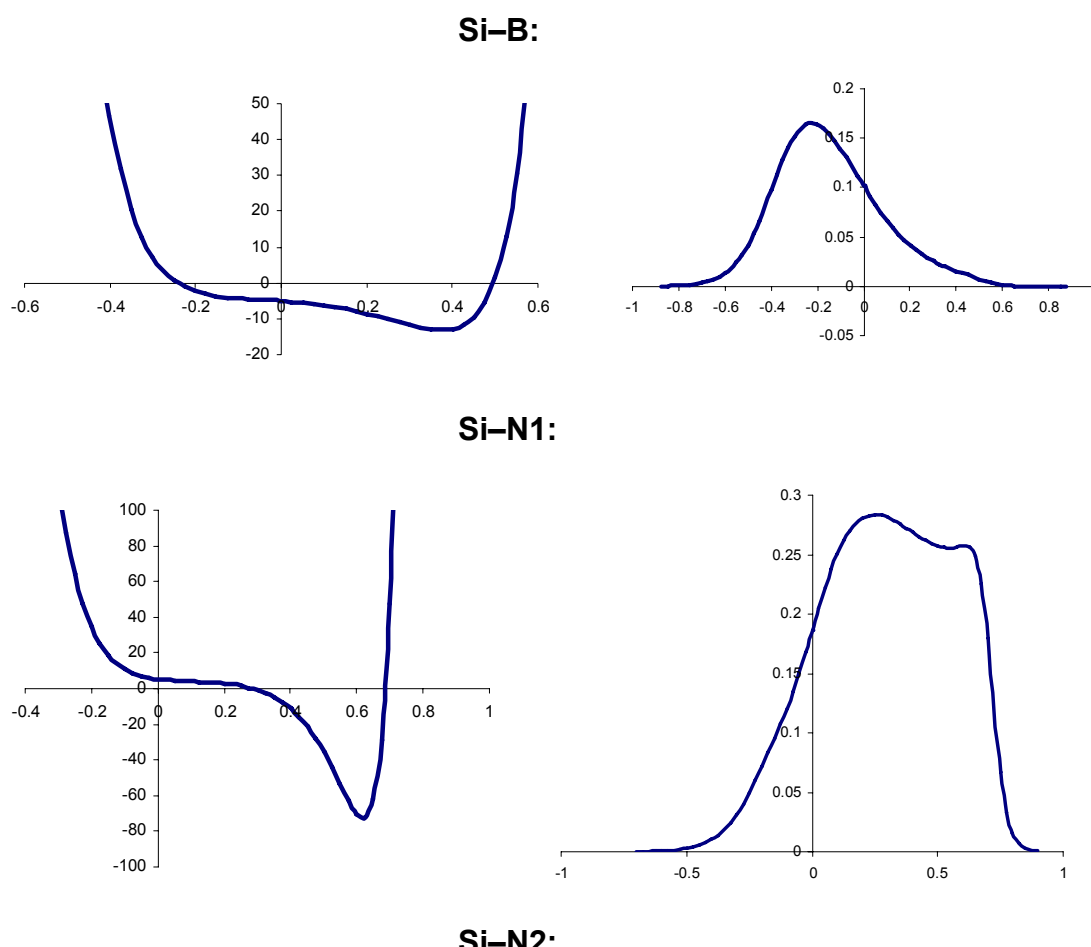
	$\rho(\mathbf{r}_{\text{BCP}})$ [eÅ ⁻³]	$\nabla^2\rho(\mathbf{r}_{\text{BCP}})$ [eÅ ⁻⁵]	λ_3 [eÅ ⁻⁵]	ε	d_{BP} [Å]	$d1_{\text{BCP}}$ [Å]	Q [e]
Si–B	0.871(25)	-5.066(41)	4.25	0.10	1.9655	0.9828	+1.68 / +1.21
Si–N1	0.826(35)	+5.172(91)	13.98	0.19	1.8430	0.8249	+1.68 / -1.31
Si–N2	0.739(31)	+6.101(86)	14.77	0.31	1.8336	0.8166	+1.68 / -1.20
N1–C8	1.751(19)	-10.205(72)	15.07	0.01	1.4754	0.8703	-1.31 / +0.48
N1–C1	2.524(28)	-21.182(143)	17.51	0.09	1.3371	0.7697	-1.31 / +0.60
N2–C1	2.418(27)	-17.641(129)	18.61	0.13	1.3455	0.7572	-1.20 / +0.60
C1–C2	1.921(24)	-13.600(72)	14.63	0.09	1.4827	0.7547	+0.60 / -0.19
C2–C3	2.058(21)	-13.843(68)	13.80	0.23	1.3963	0.7231	-0.19 / +0.06
Si–H	0.801(52)	+9.015(120)	18.24	0.50	1.4803	0.7759	+1.68 / -0.52
B–H103	1.00 (2)	+1.76 (6)	12.95	0.54	1.198	0.497	+1.21 / -0.54
B–H101/2	0.99 (1)	+0.1 (4)	10.3 (5)	0.46 (1)	1.22 (1)	0.50 (1)	+1.21 / -0.54
C _{Me} –H	1.96 (6)	+21 (2)	12.3 (3)	0.07 (4)	1.08 (1)	0.64 (2)	+0.03 / -0.02
C _{Ph} –H	1.97 (6)	+22 (2)	13.2 (7)	0.05 (2)	1.07 (1)	0.66 (1)	-0.06 / + 0.11

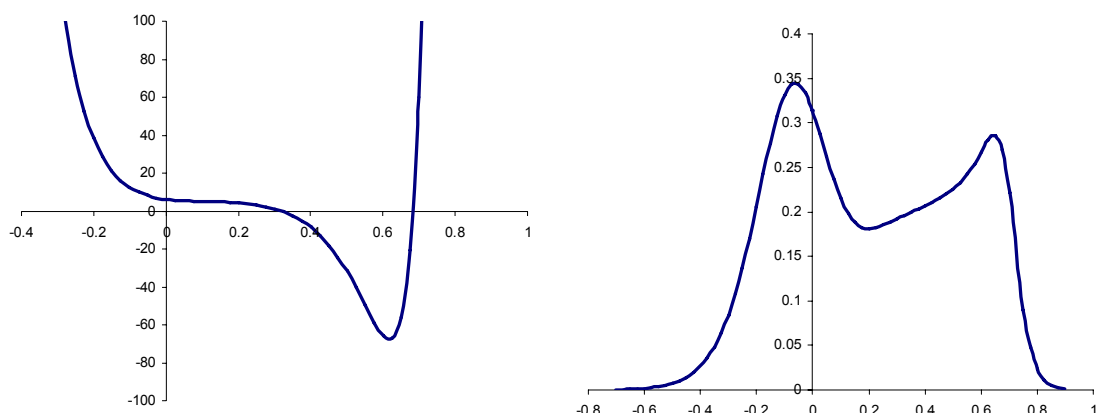
λ_3 is the curvature of $\rho(\mathbf{r})$ along the bond path, the ellipticity $\varepsilon = \lambda_2/\lambda_1-1$, d_{BP} the total length of the BP, $d1_{\text{BCP}}$ the distance of the first named atom to the BCP, Q the charge of the two involved atoms, derived by the difference of atomic number Z and $\rho(\mathbf{r})$ integrated over the atomic basin.

2.6 Bond Path Analysis

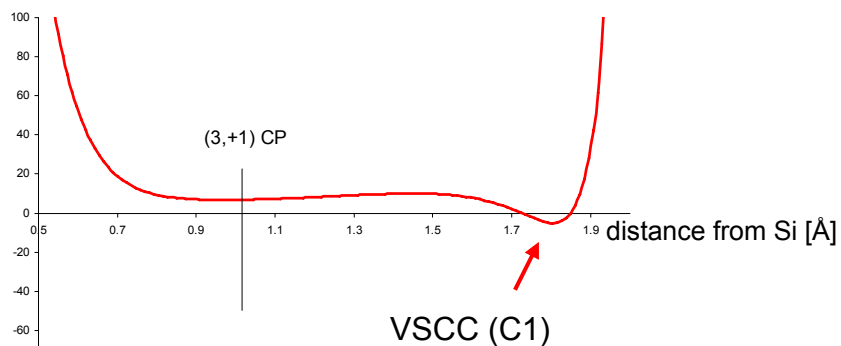
The plotted properties are the Laplacian $L(\mathbf{r}) [\text{e}\text{\AA}^{-5}]$ (left) and the ellipticity $\varepsilon(\mathbf{r})$ (right) along the bond path (BP) from the first to the second labelled atom. The y-axis (property) intersects the x-axis (distance from the bond critical point BCP [Å]) at the BCP and therefore separates the BP into basins of the first (left) and the second labelled (right) atom.

a) Silicon Bonds



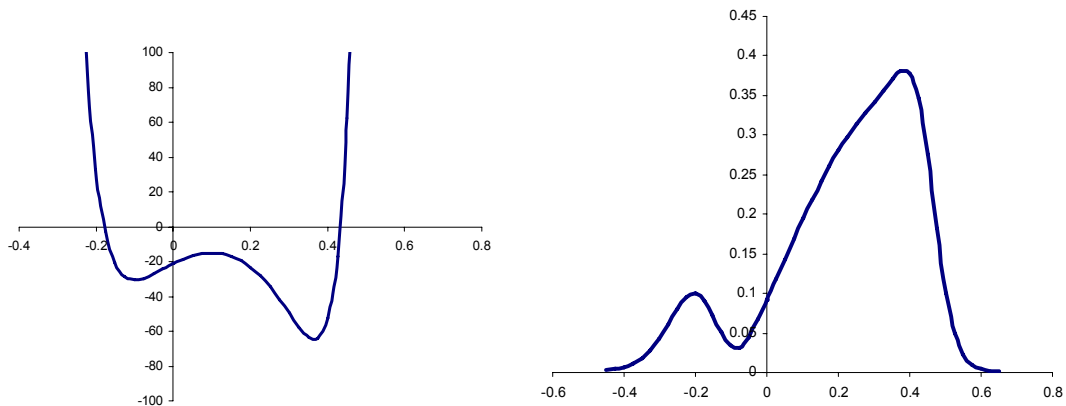


Laplacian along the line between **Si** and **C1** (no BP):

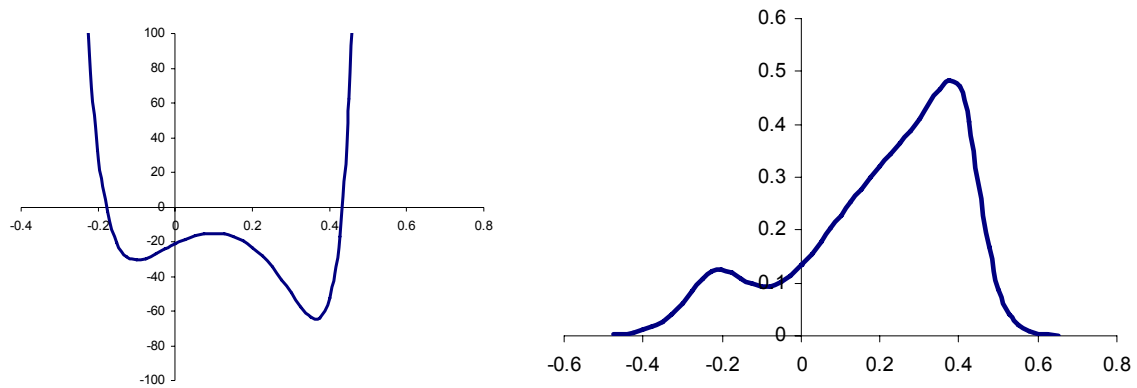


b) C–N Bonds

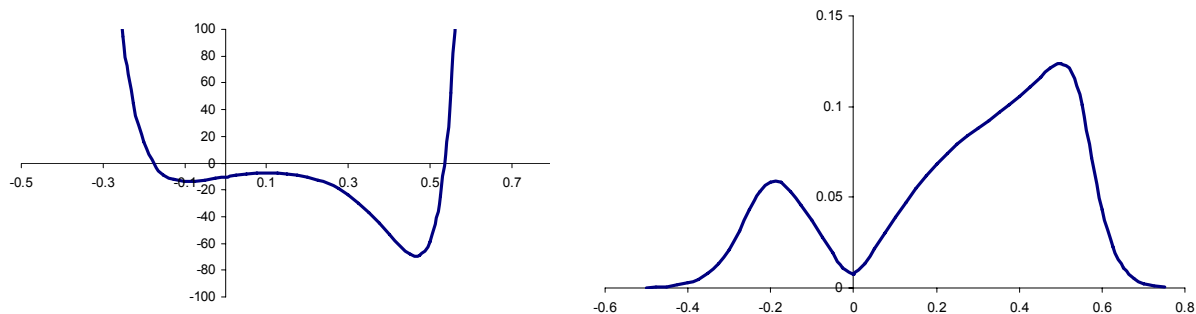
C1–N1:



C1–N2:

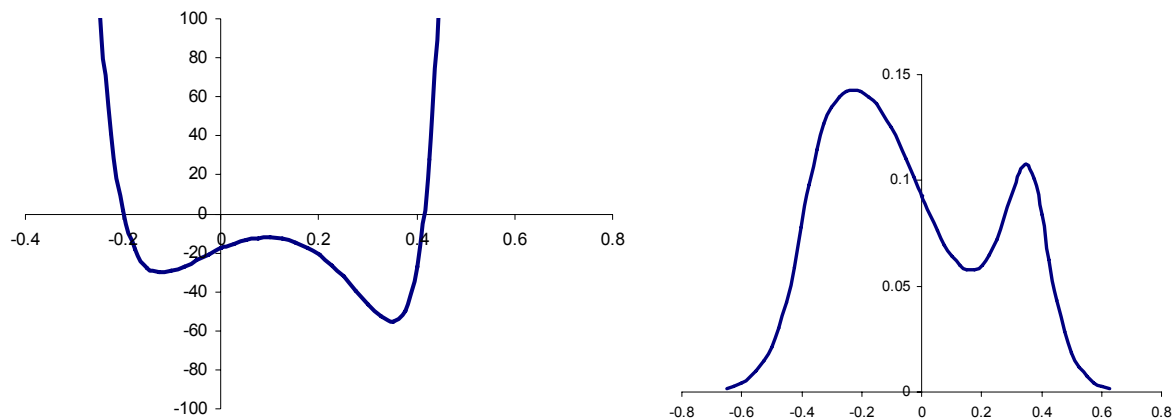


C8–N1:

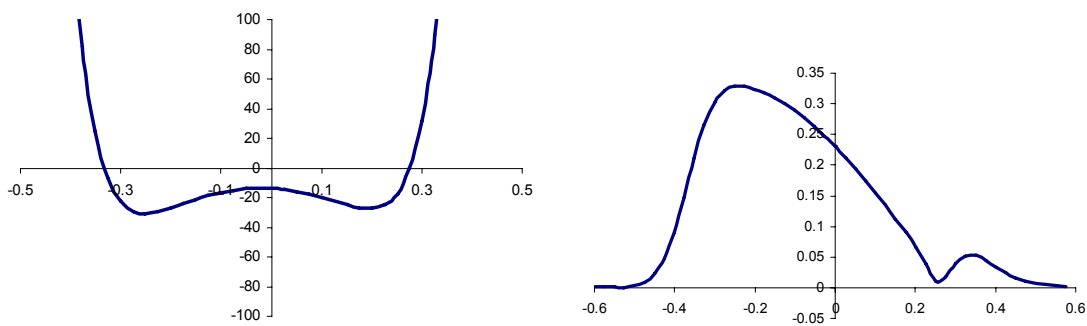


c) C–C Bonds

C1–C2:

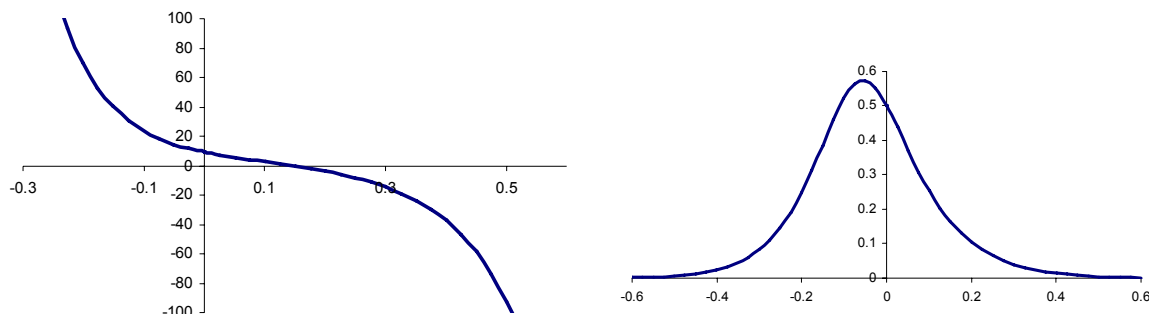


C2–C3:

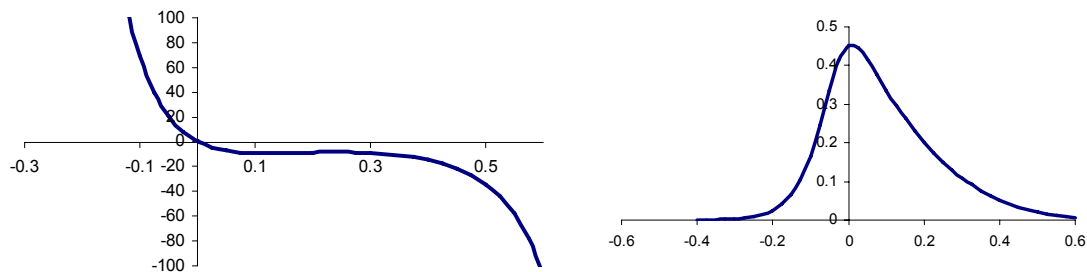


d) Hydrogen Bonds:

Si—H100:

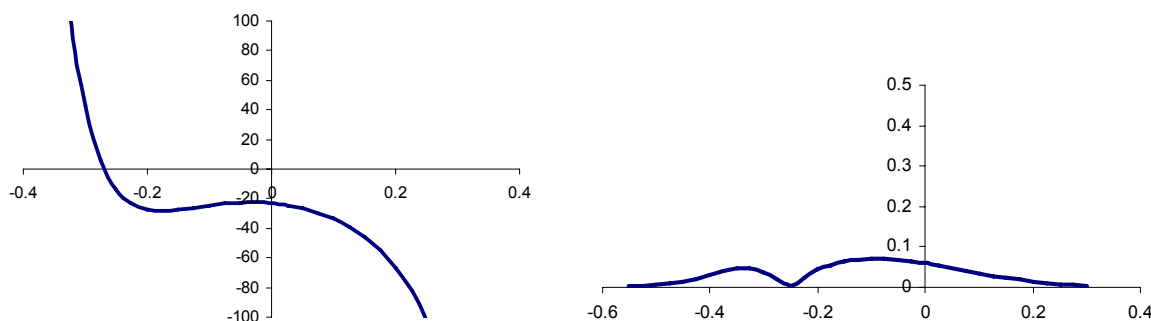


B—H:

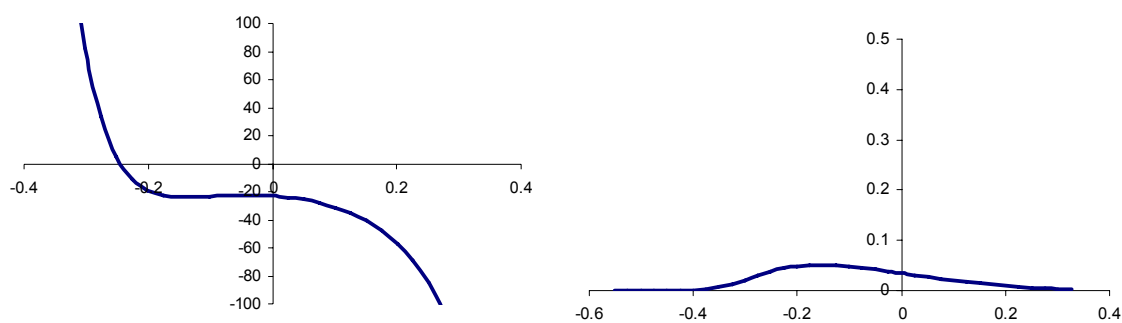


The course of $L(r)$ along B—H explains the differing values of $\nabla^2\rho(\mathbf{r}_{\text{BCP}})$ at the BCPs of the three B—H bonds. $L(r)$ changes its sign in close proximity of the BCP and pictures a steep ascent as soon as the boron-basin is reached (polarization). Therefore even small changes in the position of the BCP on the bond can lead to pronounced shifts in $\nabla^2\rho(\mathbf{r}_{\text{BCP}})$, even though the distribution of the related density is relatively flat.

C_{phenyl}—H_{phenyl} (C3—H3):



C_{methyl}—H_{methyl} (C13—H13A):



2.7 Integrated Atomic and Selected Group Charges

Table S3. The net charge is defined by the difference of the atomic number Z and the monopole population of the respective atom. The integrated charge is defined by the difference of the atomic number Z and $\rho(\mathbf{r})$ integrated over the atomic basin, defined by the zero-flux surface.

atom / group	net charge [e]	integrated charge [e]
Si	+2.077(68)	+1.680
B	-0.886(173)	+1.210
N1	-0.835(54)	-1.313
N2	-0.836(50)	-1.205
C1	+0.106(76)	+0.597
C2	-0.162(62)	-0.186
C3	+0.190(46)	+0.064
C4	+0.141(42)	-0.051
C5	+0.101(48)	-0.102
C6	+0.141(42)	-0.046
C7	+0.190(46)	+0.022
C8	+0.517(74)	+0.483
C10	+0.174(71)	+0.033
C12	+0.459(76)	+0.393
C13	+0.084(72)	+0.035
H10A	-0.091(19)	-0.028
H13A	-0.035(17)	-0.006
H100	-0.697(37)	-0.525
H101	+0.070(36)	-0.532
H102	+0.070(36)	-0.540
H103	+0.070(36)	-0.542
H3	-0.071(20)	+0.107
H4	-0.071(20)	+0.129
H5	-0.071(20)	+0.107
BH ₃	-0.676	-0.404
SiH	-1.380	+1.155
PhC(N <i>t</i> -Bu) ₂	-1.284	-0.867

On the first sight the difference between the net charge (-0.886) and the integrated charge (+1.210) of the boron atom is unexpected, but it can be understood by the severely negative integrated charges found for the bound hydrogen atoms (-0.538 in av.). The value itself corresponds to the charges found in a recent paper published by Mebs et al., where charge transfer effects in hyradzine boranes were investigated based on integrated density-based descriptors like e.g. the integrated charges.^{S15} These charges reflect the polarization of the bonding density towards the hydrogen atoms. Figure S3 shows that the BCPs of the B–H bonds are located relatively close to the boron atom, which leads to increased volumes of the hydrogen atoms and the associated charges. The net charges can not reflect these polarized charge distributions. This is one reason why we refer to group charges in addition to the atomic charges in the paper, since the group charges are more direct related to the chemistry.

2.8 Laplacian Distribution

Two-Dimensional Distribution of $L(r)$ in Selected Planes

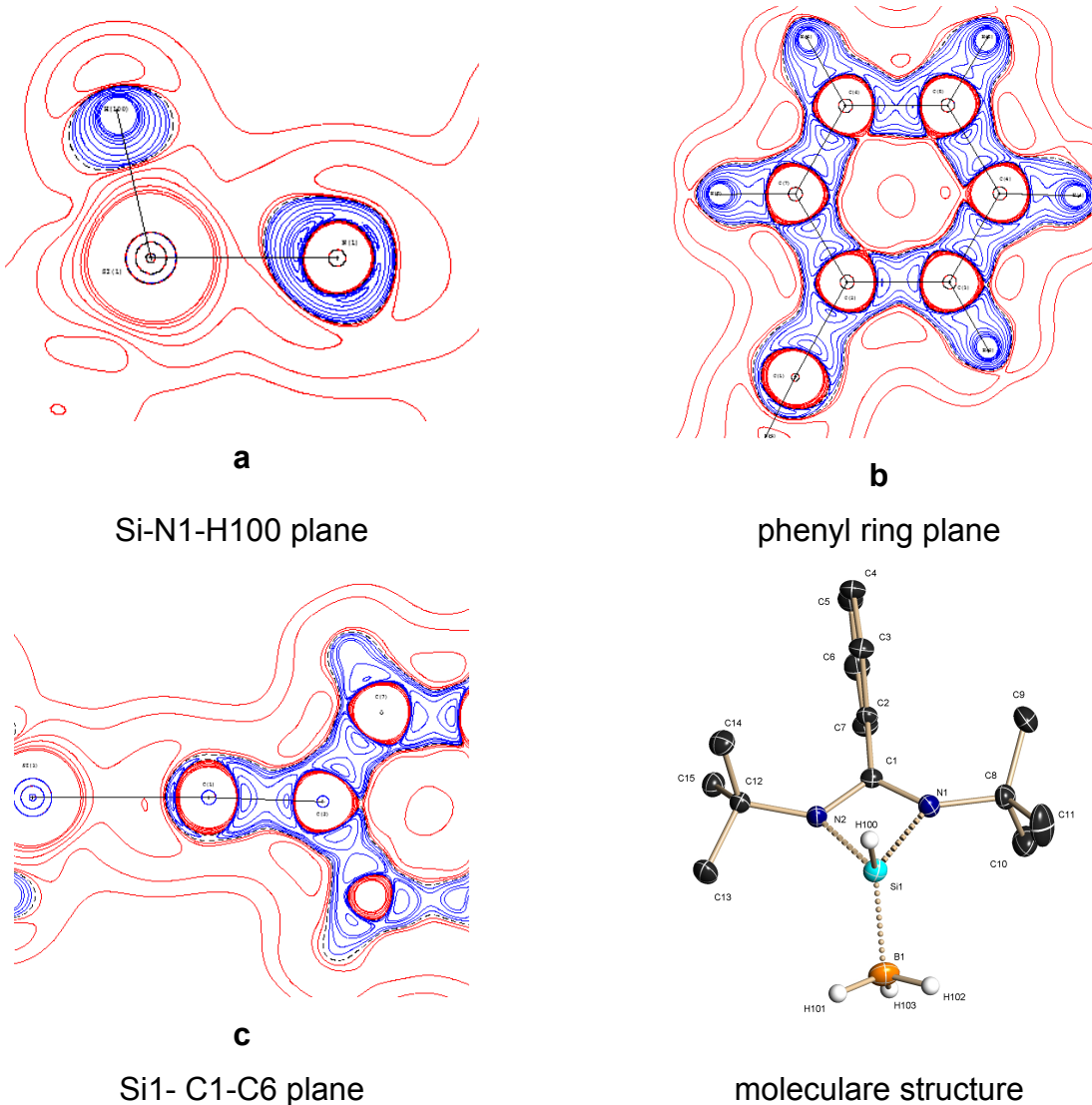


Figure S4: $L(r)$ in selected planes negative values ranging from -1 to $-70 \text{ e}\AA^{-5}$ (charge concentrations) are plotted in blue and positive values ranging from $+1$ to $+10 \text{ e}\AA^{-5}$ (charge depletions) in red contour lines.

The distributions above show the deviation from the direct connection line to the silicon atom of the lone-pair associated charge concentrations at the nitrogen atom (Figure S4a), the typical distribution for shared interactions (Figure S4b), and the charge concentration at C1 toward Si1 (Figure S4c).

Three-Dimensional Distribution of $L(r)$ on Selected Isosurface Values

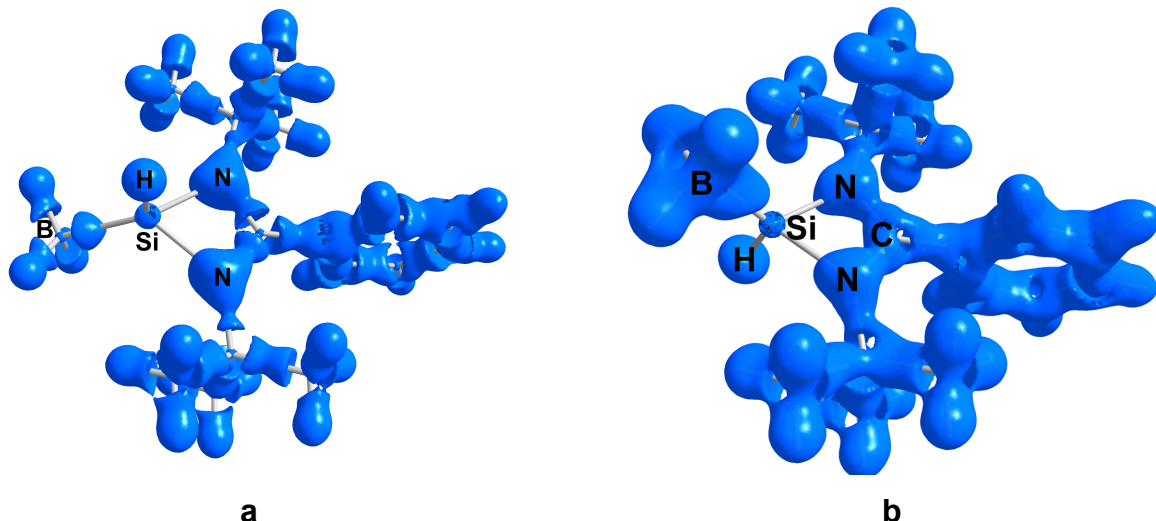


Figure S5: $L(r)$ isosurface on the $-5 \text{ e}\text{\AA}^{-5}$ level (a) and reactive surface (b), defined by $L(r) = 0 \text{ e}\text{\AA}^{-5}$.

The three-dimensional representation of the Laplacian distribution in Figure S5, b shows the extremely polar nature of the silicon bonds. With the exception of the Si–B bond all charge concentrations are located close to the bonding partners of the silicon atoms. Even the hydrogen atom is almost spherically surrounded by an area of charge concentration, which makes this hydrogen atom unique in comparison to all others in the molecule.

The reactive surface in Figure S5, b displays regions of possible nucleophilic attack. Holes in this isosurface refer to regions where the Laplacian changes sign. These are the sites where charge depletions occur.

2.9 Critical Points in $L(r)$ – Density-Based Geometrical Parameters from the Charge Concentrations (CC)

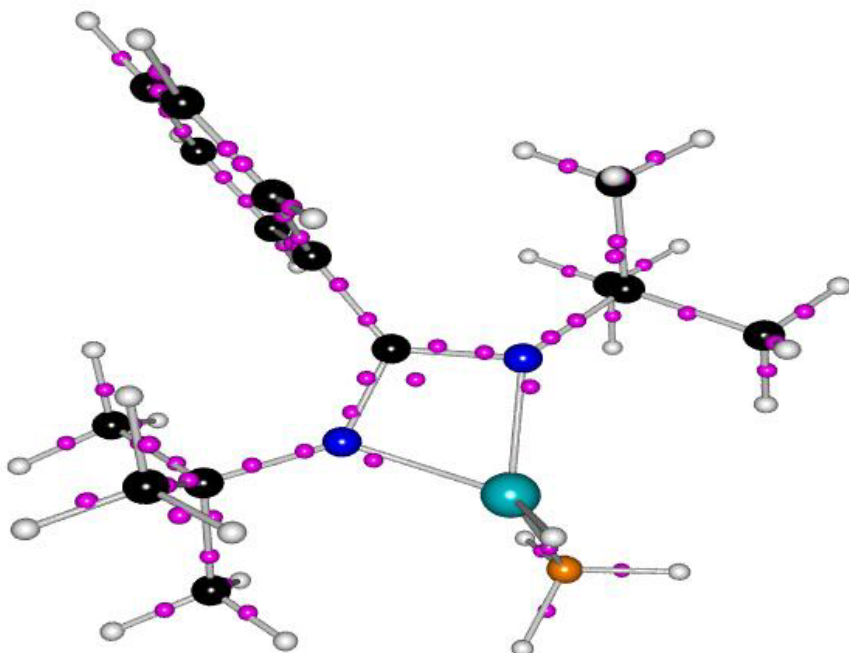


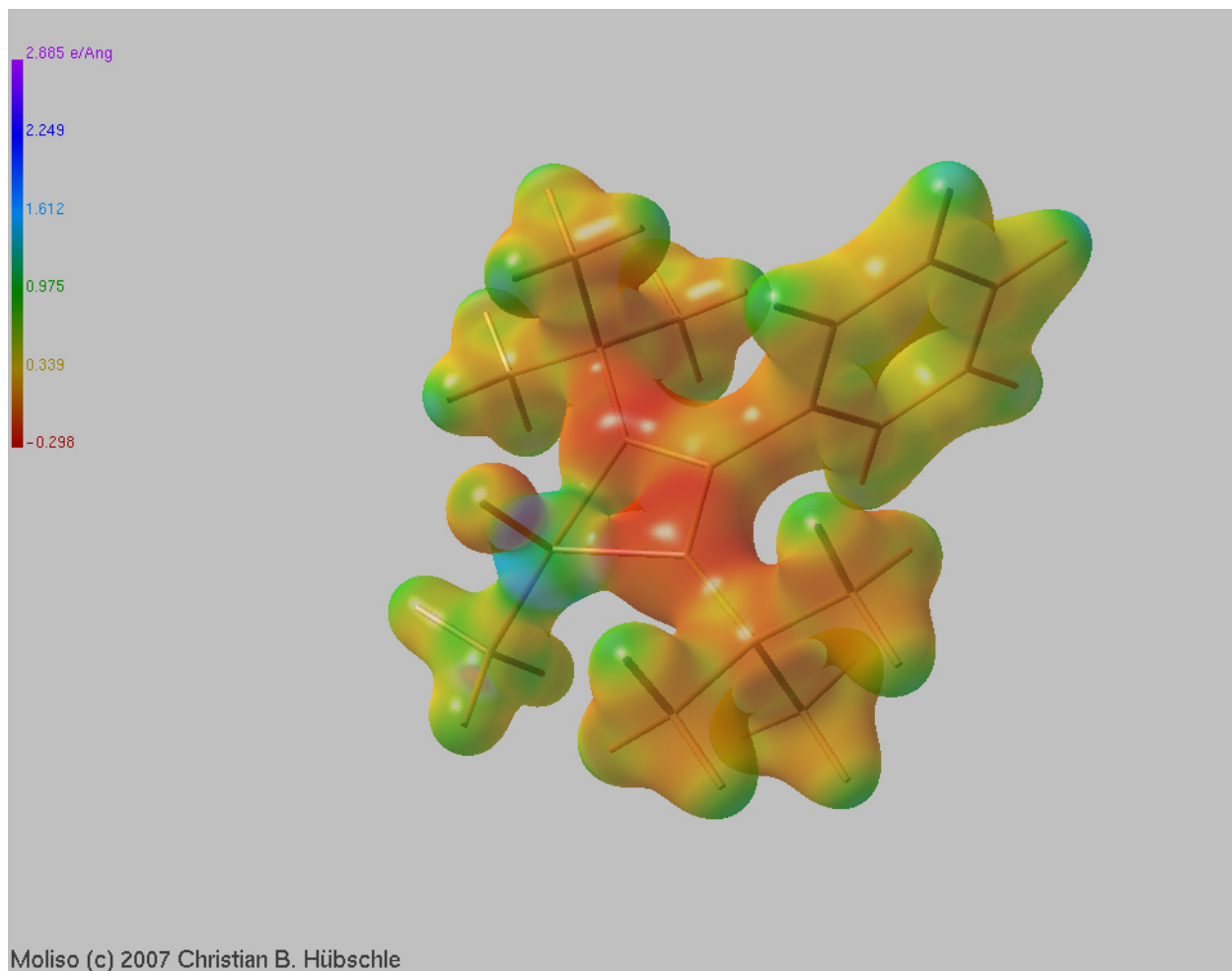
Figure S6: (3, +3) critical points in $L(r)$.

For all non-hydrogen atoms the (3, +3) critical points of $L(r)$ were determined (local minima in $L(r)$, respectively local maxima in the negative Laplacian and therefore maxima of the charge concentrations (CC) in the valence shells of the atoms, which can be associated with lone-pairs and valence shell polarizations due to bonding. These points depicted as magenta spheres were used to calculate the 'density-based geometry' of the molecule cited in the paper. A connectivity framework of these charge concentrations can give much more insight into density-based properties like hybridization or bend bonds, since it is the polarization of the valence shell which is the response of bound atoms to the interaction with the neighbouring atoms.

In a few cases the CCs were of the (3, +1) type, which means that the eigenvalue λ_1 is negative. This is due to a flat density distribution, which can cause problems in the numerical algorithms. One has to keep in mind that the fourth derivative of $\rho(r)$ has to be inspected for the determination of the critical points in $L(r)$. The atoms, where we find (3, +1) instead of (3, +3) CPs are C4 and C7 and the tertiary carbon atom C8 and the two methyl carbon atoms C9 and C11. As can be seen in Figure S1, the thermal ellipsoid of C11 indicates a marginal disorder. This probably leads to a flat density distribution and might be the reason for the lack of a (3, +3) CP there and at

the bonded C8 as well. The lack of the (3, +3) CPs at C4 and C7 might be due to the 'chemical constraint', which makes them share the same set of angular and expansion/contraction parameters. However, even if those chemical constraints (they are also applied for subsets of hydrogen and methyl carbon atoms) may cause some of the uncertainties in the fourth derivative of the fitted density, they have to be used, in order to stabilize the fit, especially in non-centrosymmetric space groups.

2.10 Electrostatic Potential



Moliso (c) 2007 Christian B. Hübschle

Figure S7: Electrostatic potential (color-coded) mapped on the isosurface representation of the electron density distribution on the $0.5 \text{ e}\text{\AA}^{-5}$ level.

The electrostatic potential (ESP) mapped on an isosurface of the electron density distribution is a useful tool to identify attractive regions for nucleophiles or electrophiles, respectively. Nucleophiles tend to attack regions with positive potential (electron depletion, blue). Sites for preferred attack of electrophiles are those with negative potential (red). As expected, we locate the area with the highest values of positive ESP at the silicon atom, and the most distinct negative values at the nitrogen atoms, but also around the silicon bonded H100.

2.11 Static Deformation Density

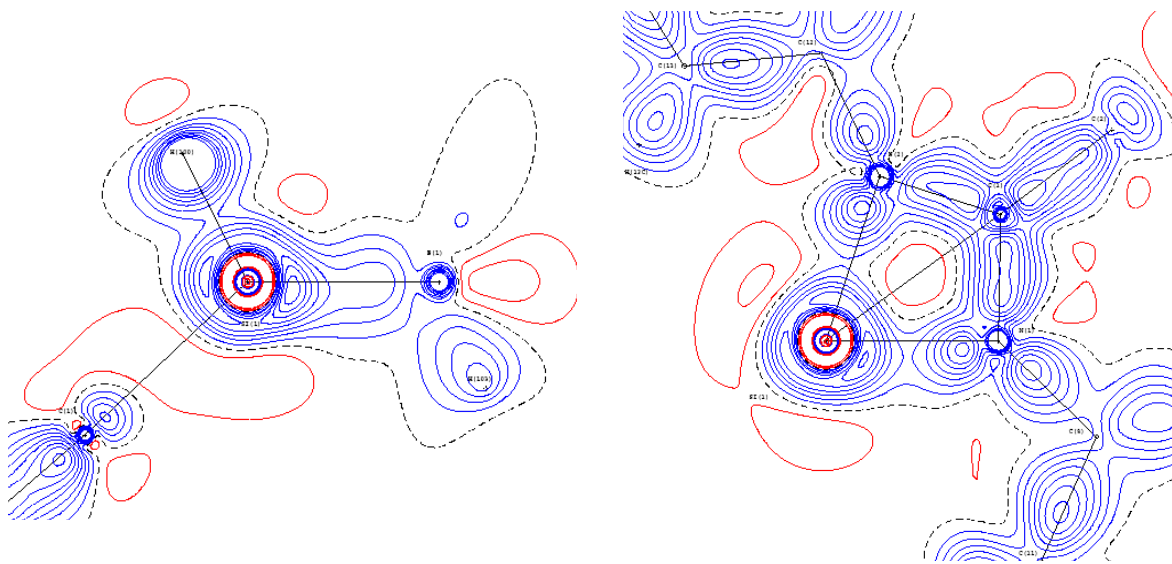


Figure S8: Static deformation density in the Si–B–H100 (left) and the Si–N1–N2 plane (right); contour intervals 0.1 eÅ⁻³.

References

- [S1] G. M. Sheldrick, SADABS 2006/3, Göttingen (Germany), **2006**.
- [S2] G. M. Sheldrick, SHELXS in SHELXTL v6.10, Madison (USA), **2001**.
- [S3] G. M. Sheldrick, SHELXL in SHELXTL v6.10, Madison (USA), **2001**.
- [S4] F. H. Allen, *Acta Crystallogr.* **1968**, *B42*, 515-522.
- [S5] P. Rademacher, *Strukturen organischer Moleküle*, VCH, Weinheim/New York, **1987**.
- [S6] N. K. Hansen, P. Coppens, *Acta Crystallogr.* **1978**, *A34*, 909-921.
- [S7] A. Volkov, P. Macchi, L. J. Farrugia, C. Gatti, P. R. Mallinson, T. Richter, T. Koritsanszky, XD2006, A Computer Program Package for Multipole Refinement, Topological Analysis of Charge Densities and Evaluation of Intermolecular Energies from Experimental or Theoretical Structure Factors, **2006**.
- [S8] a) Z. Su, P. Coppens, *Acta Crystallogr.* **1998**, *A54*, 646-652; b) P. Macchi, P. Coppens, *Acta Crystallogr.* **2001**, *A57*, 656-662.
- [S9] a) E. Clementi, D. L. Raimondi, *J. Chem. Phys.* **1963**, *38*, 2686-2689; b) E. Clementi, C. Roetti, *Atom. Data Nuc. Data Tab.* **1974**, *14*, 177-478.
- [S10] N. Kocher, J. Henn, B. Gostevskii, D. Kost, I. Kalikhman, B. Engels, D. Stalke, *J. Am. Chem. Soc.* **2004**, *136*, 5563-5568.
- [S11] A. Volkov, Y. A. Abramov, P. Coppens, *Acta Crystallogr.* **2001**, *A57*, 272-282.
- [S12] F. L. Hirshfeld, *Acta Crystallogr.* **1976**, *A32*, 239-244.
- [S13] H. D. Flack, *Acta Crystallogr.* **1983**, *A39*, 876-881.
- [S14] K. Meindl, J. Henn, *Acta Crystallogr.* **2008**, *A64*, 404-418.

[S15] S.Mebs, S. Grabowsky, D. Förster, R. Kickbusch, M. Hartl, L. L. Daemen, W. Morgenroth, P. Luger, B. Paulus, D. Lentz, *J. Phys. Chem. A* **2010**, *114*, 10185-10196.